A&A 585, A40 (2016)
DOI: 10.1051/0004-6361/201526620

Astronomy & Astrophysics

Reconstructing solar magnetic fields from historical observations

I. Renormalized Ca K spectroheliograms and pseudo-magnetograms

Alexei A. Pevtsov[1], Ilpo Virtanen[2], Kalevi Mursula[2], Andrey Tlatov[3], and Luca Bertello[4]

[1] National Solar Observatory, Sunspot, NM 88349, USA
e-mail: apevtsov@nso.edu
[2] ReSoLVE Centre of Excellence, Astronomy and Space Physics research unit, University of Oulu, POB 3000, 90014 Oulu, Finland
e-mail: [ilpo.virtanen;kalevi.mursula]@oulu.fi
[3] Kislovodsk Mountain Astrophysical Station of Pulkovo Observatory, PO Box 145, Gagarina Str. 100, 357700 Kislovodsk, Russian Federation
e-mail: tlatov@mail.ru
[4] National Solar Observatory, 950 N. Cherry Avenue, Tucson, AZ 85719, USA
e-mail: lbertello@nso.edu

Received 27 May 2015 / Accepted 28 October 2015

ABSTRACT

Aims. The present work is the first in a series of articles that develop a new proxy to represent the evolution of magnetic activity in past solar cycles by combining the information from historical Ca II K line spectroheliograms and sunspot magnetic field measurements.
Methods. We use synoptic (Carrington) maps from 1915–1985 that were derived from daily Ca K line observations at Mount Wilson Observatory to identify the chromospheric plages and to create synoptic pseudo-magnetograms. We use historical observations of sunspot magnetic fields from 1917 to the present to assign polarity to pixels situated within plages. The original Ca K spectroheliograms are nonuniform in their brightness, and we develop a novel approach to re-normalize their intensities.
Results. We show that a homogeneous long-term series of pseudo-magnetograms can be successfully constructed by combining sunspot field measurements and plages with renormalized intensities. In our tests, about 80% of pixels situated within plages showed the same magnetic polarity as the synoptic magnetograms taken with the Kitt Peak Vacuum Telescope. Finally, we discuss possible approaches to further improve the agreement between observed and pseudo-magnetograms.

Key words. Sun: faculae, plages – Sun: magnetic fields – Sun: activity – sunspots

1. Introduction

Magnetic fields form the foundation for all active-Sun phenomena from tiny G-band bright points to sunspots and coronal mass ejections (CMEs). They serve as a reservoir of energy for flares, play a critical role in triggering mechanisms for CMEs, and provide the means of transporting energy from the photosphere to the corona. The origin of magnetic fields lies in the solar (stellar) dynamo, which still remains an enigma of solar and stellar astrophysics.

Numerous studies have been conducted in the attempt to develop a robust prediction of future solar cycles (e.g., Petrovay 2010; Tlatov & Pevtsov 2010; Pesnell 2014; Pishkalo 2014, and references therein). While these predictions are still unreliable, related studies have identified parameters that seem to be important for predicting the strength of the solar cycle (Petrovay 2010; Hathaway 2010; Upton & Hathaway 2014). One of these parameters is the strength of the polar magnetic field.

Direct measurements of the solar magnetic field started in 1917 with measurements of the sunspot field strength at Mount Wilson Observatory (MWO; Hale et al. 1919). The first magnetographic observations date back to the late 1950s, with routine synoptic observations of full-disk magnetograms starting in the early 1970s. The full-disk magnetograms also provide the most complete information about polar fields, although some limited information can be inferred from the surface distribution of certain photospheric and chromospheric structures (e.g., polar crown filaments may outline the location of the lower boundary of a polar unipolar field, Babcock & Babcock 1955; Hyder 1965). One of the proxies of magnetic fields – the brightness of the chromospheric Ca II K 393.37 nm spectral line – is available in the form of full-disk images (spectroheliograms) of the Sun. The earliest synoptic Ca II K line spectroheliograms were measured in 1907 at Kodaikanal Observatory in India (Foukal et al. 2009).

The correlation between bright chromospheric plages observed in Ca II K spectral line and unsigned magnetic flux was noted from the very beginning of magnetographic observations (Babcock & Babcock 1955; Leighton 1959; Stepanov & Petrova 1959). Figure 1 provides an example of a synoptic map in the Ca II K line and a magnetogram for Carrington rotation (CR) 1708. The bright areas in the Ca II K line map spatially correspond very well with the areas of identifiable magnetic fields in the magnetograms. This correspondence is clear for areas with a strong magnetic field (active regions) as well as for the weaker, more dispersed fields of decaying active regions. The relation between the magnetic flux density and the intensity of the Ca K line is nonlinear. For example, areas with the strongest magnetic field (sunspot umbrae) appear as dark voids in the middle of bright plages (see two examples indicated by arrows in Fig. 1). The correlation between the intensity in the Ca K line core and the magnetic flux density is made complex by several factors, including center-to-limb variation, different dependency for different structures, and nonlinearity (see, Harvey & White 1999,

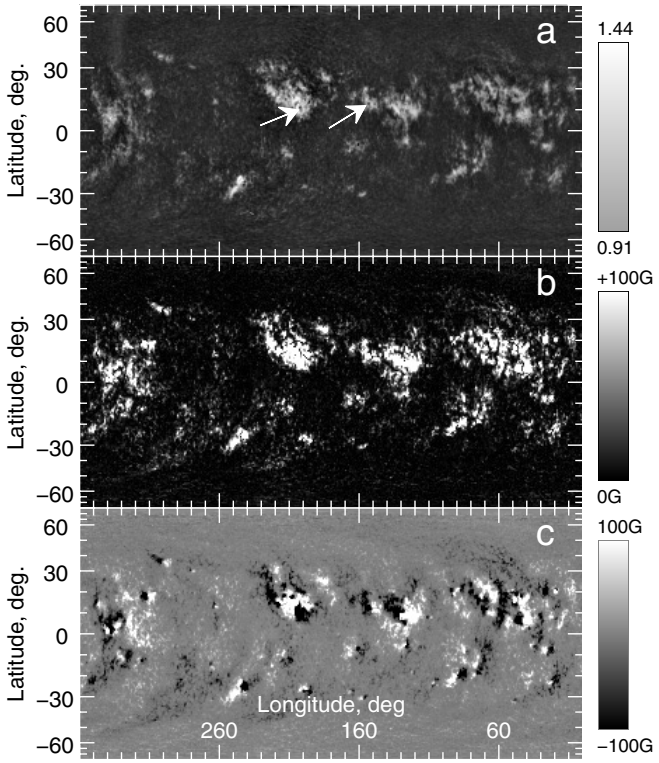

Fig. 1. Synoptic maps of the Ca K-line intensity (*upper panel*), unsigned (*middle*), and signed (*lower panel*) magnetic flux for CR1708. In the magnetogram (*lower panel*) the black and white halftones correspond to magnetic fields with negative and positive polarity. The Ca K-line observations are taken from the MWO, the magnetic field data from the NSO/KP. Two arrows point to dark circular voids (corresponding to sunspot umbrae) in the middle of bright plages. Panel **c)** is scaled between ±100 G (see scale on the right side of the panel).

and references therein). On the other hand, proxies representing integrated properties of chromospheric plages seem to correlate quite well with the magnetic flux (Tlatov et al. 2009).

The present work is the first in a series of articles that attempt to develop a new proxy to represent the evolution of magnetic activity in past solar cycles by combining the information from historical Ca II K line spectroheliograms and sunspot magnetic field measurements. In this article we first revisit the relationship between magnetic flux and the CaK line intensity (contrast) using the Ca K line and observations of the sunspot magnetic field at the MWO and magnetograms from the National Solar Observatory at Kitt Peak (NSO/KP; the data sets are described in Sect. 2). Then, we discuss the normalization of the Ca II K-line data (Sect. 3) and combine plage information derived from Ca K spectroheliograms with the polarity of magnetic fields from MWO sunspot field strength measurements to create pseudo-magnetograms (Sect. 4). In Sect. 5 we discuss our results.

2. Data

The data used in this paper include the synoptic maps of Ca II K-line normalized intensities and the magnetic flux density and polarity of strong magnetic fields in sunspots.

2.1. Ca K line synoptic maps

Synoptic maps of the normalized intensity of the Ca II K line have been derived from daily full-disk spectroheliograms taken at Mount Wilson Observatory from August 1915 to July 1985 (Hale 1908; Ellerman 1919). The spectroheliograms were recorded on a photographic medium (first on plates and later on film) with a spectral bandpass of about 0.035 nm in width (this width takes into consideration the diffraction at the exit slit; the uncorrected exit slit used in observations is 0.02 nm). The optical format (four images per plate) and photographic plate material remained mostly the same until October 8, 1962. On that date the diameter of the solar image size increased from 2 inches to 3.4 inches, and two images were recorded on the same plate. The glass thickness also decreased as part of the change. Photographic plates were replaced by the much cheaper films in February 1980.

The visual appearance of the MWO data is not uniform. Images from the mid-1950s to the mid-1960s show the chromospheric filaments much more clearly than data of other periods. Tlatov et al. (2009) and Bertello et al. (2010) also noted the increase in contrast of images during the same period of time. No detailed description of the daily observations exist, but it was speculated that this change in contrast might be related to the use of a narrower exit slit when taking the spectroheliograms. Cursory examination of observation logbooks[1] indicates that in early observations (1915–1920), the spectrograph entrance slit (the so-called first slit) was set to 0.1–0.15 mm (which corresponds to approximately 3.5–5.3 arseconds for a 2-inch image of the Sun). The width of the spectroheliograph exit slit (the so-called A-slit, or second slit), which selects the wavelength band to be recorded on a photographic plate, was 0.15 mm. The instrument description by Ellerman (1919) cites 0.1/0.15 mm (first/A-slit) for K-line observations. Logbooks in 1927 and 1928 list various slit widths (0.1 mm/0.1 mm, 0.15/0.15, 0.12/0.12 and 0.14/0.12). Since late 1928, the majority of observations are taken with 0.1/0.1 mm slit widths. Records of observations taken in 1931 still show occasional observations with 0.1/0.12 mm slit widths. In February 1932, the logbook format was changed, and the slit width was not recorded for each observation. A general note for the 1932 logbook states that the slit widths used for K-line observations are 0.1/0.1 mm. The 1950 logbook gives the slit widths as 0.0035/0.0055 inch, which corresponds to 0.09/0.14 mm – slightly wider than the slit width in 1930. The 1959 logbook contains a note that for 2-inch images of the Sun the slits were set to 0.07/0.07 mm. Since the diameter of solar images on spectroheliograms was about 2 inches at that time, this note seems to support the notion that the data were taken with narrower exit slits (0.07 mm vs. 0.1−0.15 mm in early periods). Unfortunately, the spectrograph exit slit in later periods is less well recorded. The 1961 and 1964 logbooks contain notes that might be interpreted as if a much greater exit-slit width was used in later periods (e.g., the 1964 logbook records "offset for K2, set 2nd slit on D1 (5896), increase micrometer reading 3.19 mm"). Finding more details about the slit widths used in different periods of time would require a more detailed (and time-consuming) examination of the logbooks, but this information is not essential for the purpose of this work.

Thus, the nonuniformities in Ca II K line images can be attributed to changes in the observation setup (e.g., larger image sizes after October 8, 1962, changes in the thickness of the photographic plates, the switch from glass plates to film,

[1] See ftp://howard.astro.ucla.edu/pub/obs/spectroheliogram_logbooks/

and finally, changes in entrance and exit spectroheliograph slits). Before October 9, 1961, the Ca II K image did not have a calibration wedge imprinted on plate, which prevents a proper intensity calibration of these data. Bertello et al. (2010) developed an alternative flatfielding routine for observations without a calibration wedge. In this study, we use data that were flatfielded and intensity-normalized as given by Bertello et al. 2010. The intensities in these maps are normalized to the mean chromospheric intensity (which is set to unity); normalized intensities above one correspond to areas that are brighter than the mean chromosphere.

2.2. Magnetic field measurements

The earliest measurements of the field strength in sunspots date back to 1915, with systematic observations starting in 1917 at Mount Wilson Observatory. The magnetic field strength was measured by the observer who would visually find the displacement between two Zeeman components of a spectral line (for a detailed description of this technique, see Pevtsov et al. 2011). Initially, the observations were taken in the spectral line Fe I 617.3 nm (Landé factor = 2.5). Beginning in October 1961, the spectral line was changed to Fe I 525.0 nm (Landé factor = 3.0). To accommodate a larger displacement, the glass tip-plate in the measuring micrometer was replaced with a thicker one. This change increased the nonlinearity between the angle of tip-plate and the lateral displacement, and it also imposed an upper limit on the amplitude of the magnetic fields that could be measured. Other changes included the replacement of spectral gratings with slightly different characteristics and undocumented changes in the spectrograph entrance slit. The sunspot field strengths are written in by hand on the daily drawings[2].

The total number of drawings is about 26 000. As part of the digitization project, we tabulated several parameters from the drawings, including the field strength and polarity for all measured sunspots (Tlatov et al. 2015). The changes in observations described above may affect the measurements of field strengths. Since not all of these effects are clearly understood as yet, in the present article we only employ the polarity of magnetic field, not the field strength.

To establish the scaling between the intensity in Ca II K line and the magnetic flux density, we employed synoptic magnetograms from the Kitt Peak Vacuum Telescope (KPVT, see Livingston et al. 1976), which is operated by the National Solar Observatory. This data set covers 1973–1985 and is available via NSO/SOLIS web site[3]. Figure 1 provides an example of the two synoptic maps (Ca II K line and a magnetogram).

3. Improving the Ca K line data

As noted above, the mean intensity in the synoptic maps of the Ca II K line is evidently nonuniform. This nonuniformity is clearly visible in the distribution of intensities in Ca K synoptic maps. Figure 2 shows a 2D intensity histogram in the range of 0.9−1.5. In this data set the intensity of image background is set to unity (Bertello et al. 2010). The distribution of intensities for the entire data set is shown in Fig. 2 (upper right panel). For the following discussion we loosely define the "core" of the distribution as inner part of the peak intensity; in the color bar used in Fig. 2 (upper left panel), the core is shown approximately by yellow and bluish colors, and red corrosponds to the tail of the distribution. The intensity distributions computed for separate Carrington rotations exhibit several distinct properties. The tail of the distributions shows a notable enhancement associated with solar cycle maxima (red extends to lower boundary of the 2D histogram in Fig. 2, upper left panel). The core of distributions (blue and yellow in Fig. 2 upper left panel) is quite broad in early years. It broadens significantly during cycle 19 and becomes significantly narrower in 1982–1983. This broadening in the distribution core in cycle 19 coincides with the period of increased contrast in MWO images, presumably associated with observations taken with the narrower spectrograph slit (see Sect. 2).

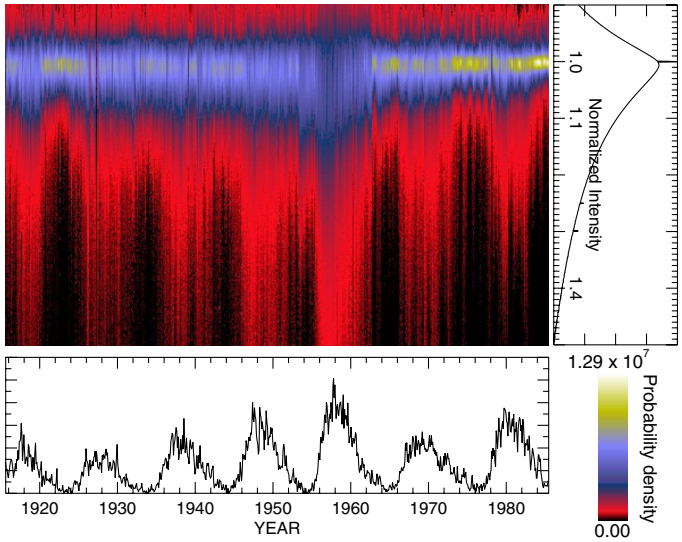

Fig. 2. *Upper left*: 2D histogram of normalized intensities computed for each Carrington rotation. The upper part of the plot corresponds to intensities of 0.9, the lower part to a normalized intensity of 1.5. *Upper right*: distribution of normalized intensities for all data sets. For reference, the *lower panel* shows the monthly international sunspot number. The horizontal axis for the *upper right panel* is the same as in *the lower panel*. The sharp peaks in the distribution of normalized intensities (*upper right panel*) at about 1 and about 1.3 are artifacts caused by missing data (whose intensity was set to unity) and erroneous data. The color bar in the lower right corner shows the scaling used for the 2D histogram in the upper left corner.

The core of distributions shows sharp quasi-annual variations, which manifest themselves as periodic peaks in the distributions (Fig. 2, upper left panel during 1965–1980). The average intensity of the synoptic maps varies around 1.015, with a slight upward trend from about 1.010 in CR827 (July–Aug. 1915) to 1.020 in CR1300 (Nov.–Dec. 1950). During cycle 19, the mean intensity rises sharply to 1.06–1.07, and between CR1400 (May 1958) and CR1450 (Jan.–Feb. 1962), it falls to about 1.005–1.010. The standard deviation of the mean intensities shows a similar pattern with $\sigma \approx 0.3$–0.4 in CR827–1300, a sharp rise to $\sigma \approx 0.9$–1.5, followed by a decrease between CR1400 and 1450 to $\sigma \approx 0.15$–0.2. These long-term trends in the average intensity and their standard deviation further support the nonuniformity in the original Ca K line synoptic data from MWO.

According to several researchers (e.g., Harvey & White 1999), the intensity distributions of Ca K line images can be interpreted as a combination of quiet-Sun and active-Sun components. The contribution of active-Sun component takes the form of an increase in the number of brighter features, which enhances

[2] ftp://howard.astro.ucla.edu/pub/obs/drawings
[3] http://solis.nso.edu

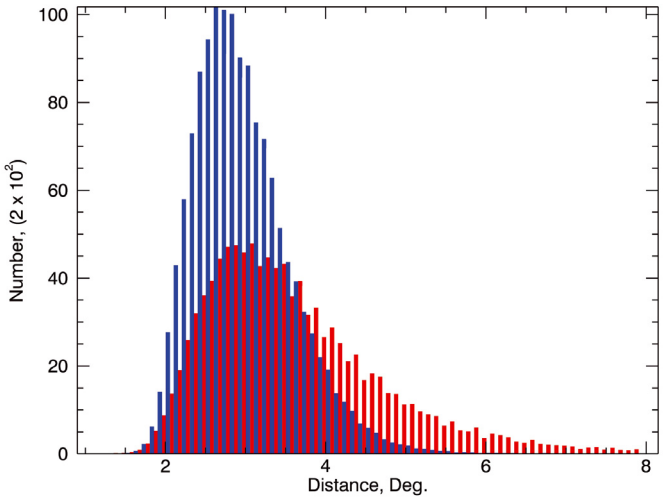

Fig. 3. Distribution of spatial frequencies (sizes) detected through periodogram analysis in Ca K-line synoptic maps (blue) and magnetograms (red) for the entire MWO data set (Carrington rotations 827–1763) using rows corresponding to ranges of latitudes within ±75 degrees.

the wing of the distribution. It is currently not expected that the quiet-Sun component of the Ca K line distribution would vary in time. We now consider a possible origin of this quiet-Sun component in the Ca K line images.

3.1. Origin of small-scale structures in Ca K images

Normalized Ca II K line synoptic maps show a granular pattern of small-scale features (brightenings) distributed more or less uniformly in areas outside plages. The fluctuations in contrast between bright and dark features in the pattern is about ±2−4% relative to the mean level of brightness; the most typical values are ±1%. The pattern is present both at high latitudes and in the active region belt. The pattern is also present at different phases of the solar cycle. To further investigate the origin of this pattern, for each solar rotation in our data set we subjected individual rows of the synoptic maps (for a given latitude, all values corresponding to longitudes from 0–360 degrees) to a periodogram analysis. MWO synoptic maps have a spatial sampling of 0.5 degree, and large-scale intensity variations were removed by subtracting a five-point running average. The strongest peak (spatial periodicity) was determined using a Lomb-normalized periodogram analysis. The distribution of spatial frequencies (sizes) determined in this way is shown in Fig. 3. We also subjected the NSO/KP magnetograms to this analysis. Both Ca K synoptic maps (Fig. 3, blue) and unsigned magnetograms (red) show maxima close to the typical size of a chromospheric network (2.4 solar degrees, or 30 000 km). Magnetograms have a more asymmetric distribution (more large features in the tail of the distribution). We would would like to note that while the synoptic maps may not be the optimal data for studying the geometric properties of the chromospheric network, the data are sufficient to detect typical sizes corresponding to a supergranulation scale.

Based on this analysis, and since CaK emission is sensitive to the magnetic field, it is reasonable to assume that the small-scale structure in the CaK synoptic maps represents the chromospheric network. With this established, the core of the quiet-Sun distribution of the Ca K line intensity in Fig. 2 is expected to have very little variation from one Carrington rotation to the other.

3.2. Renormalization of Ca K line synoptic maps

Assuming the quiet-Sun contribution to be constant offers a way to recalibrate the intensities in the original Ca K line synoptic maps. We took an approach that scales the cores of quiet-Sun distributions from different Carrington rotations to a standard distribution. We investigated different types of distributions that fit best the observed intensity distribution for the original Carrington maps. The best fits were most of the time found with T location-scale and generalized extreme value functional distributions, but some rotations are best matched using a normal or lognormal distribution. We compared different fits based on the Bayesian information criterion (BIC), which basically describes the goodness of the fit and also takes into account the number of free parameters in the fitting. We found that the best distribution function describing the whole Carrington map is not the normal distribution. However, the normal distribution fitted to the core of the quiet-Sun distribution gives lower BICs (better fit) than any fit to distributions of the whole data. We divided the data into quiet-Sun and plage components rotationally by using a threshold of median plus 2σ (standard deviation). Moreover, the general pattern is that the best agreements (lowest BICs) are reached during solar minimum times, when the tail of high values in the distribution is the smallest.

Since a normal (Gaussian) distribution represented the core of the intensity distributions for all Carrington rotations sufficiently well, we decided to employ the mean $\overline{I(\varphi,\lambda)}$ and standard deviation σ to renormalize the intensities in each Carrington rotation to some common standard mean and standard deviation as

$$I^{\rm n}_{\rm cr}(\varphi,\lambda) = (I^{\rm o}_{\rm cr}(\varphi,\lambda) - \overline{I_{\rm cr}(\varphi,\lambda)}) \cdot \frac{\sigma_{\rm cr1708}}{\sigma_{\rm cr}} + \overline{I_{\rm cr1708}}, \quad (1)$$

where $I^{\rm o}_{\rm cr}$ and $I^{n}_{\rm cr}$ are the original and renormalized intensities for each Carrington rotation, and φ, λ are latitude and longitude of the pixels in the Carrington maps. All rotations were normalized to the mean, $\overline{I_{\rm cr1708}}$, and standard deviation, $\sigma_{\rm cr1708}$, of Carrington rotation CR1708 (Apr.−May 1981). Figure 4 shows the results of this renormalization. The cores of the quiet-Sun distributions are now normalized to a standard. Sharp annual variations in the cores of the quite-Sun distributions are still present, but they are significantly reduced in amplitude. The solar cycle variations in the wings of distributions are preserved, but their amplitude is also scaled accordingly. The renormalized data also show some effects that were masked in the original data set. For example, the amplitude of the quiet-Sun component in individual distributions (for individual Carrington maps) exhibits a slight solar cycle variation with the number of pixels, with an intensity close to the quiet-Sun level being 10–15% higher at solar minima than at solar maxima. This is also clearly shown in the right panel of Fig. 4 (the peak in the blue line is slightly higher than the peak in the black line), although the small size of the image makes this difference hard to see. The most obvious difference to the original distribution (Fig. 2) is the enhanced number of pixels with high brightness in the wing of the distribution around solar maxima. The visual comparison of the distributions (Fig. 4, upper right panel) with the distributions reported in Harvey & White (1999) suggests that the distribution corresponding to the minimum of the solar cycle between cycles 21 and 22 (blue line) includes structures that were identified as quiet and weak network by Harvey & White (1999). The distribution for the maximum of cycle 21 (black line) is reminiscent of plage and active region components as defined by these authors.

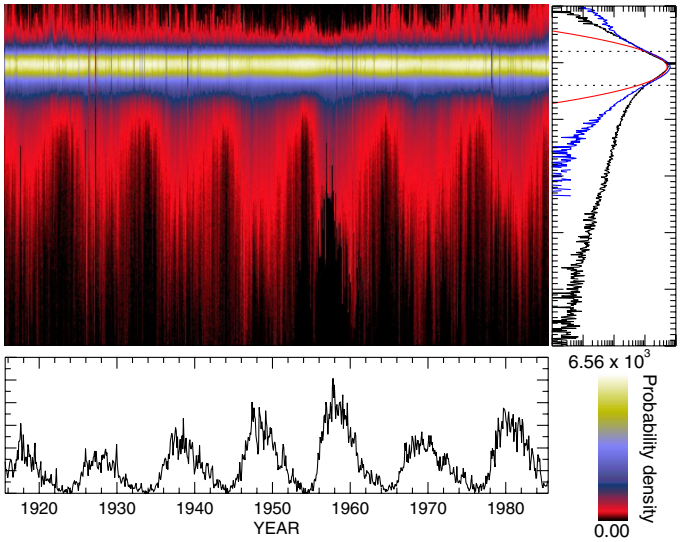

Fig. 4. *Upper left*: 2D histogram of normalized intensities computed for each Carrington rotation after the rescaling. The upper part of plot corresponds to intensities of 0.9, the lower part is at the normalized intensity of 1.5. *Upper right*: distribution of normalized intensities for CR1690 (black line, maximum of cycle 21) and CR1753 (blue, minimum between cycles 21 and 22). The red line shows a Gaussian fit to the core of the distributions. For reference, the *lower panel* shows the monthly international sunspot number. The horizontal axis for the *upper left panel* is the same as in the *lower panel*. The two dotted lines mark the approximate location of the core of the distribution used for the Gaussian fit. The vertical axis in upper right corner of the plot is the same as in Fig. 2. The color bar in the lower right corner shows the scaling used for the 2D histogram in the upper left corner.

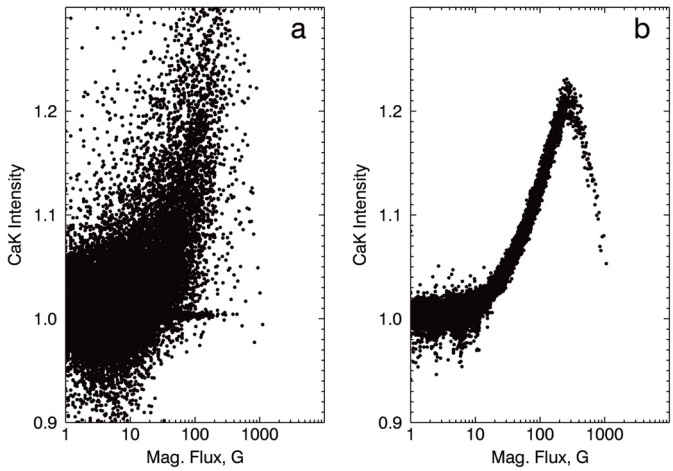

Fig. 5. Scatter plot of the magnetic flux density as a function of intensity in the Ca K-line. **a)** Pixel-by-pixel correlation for 62 000+ data points from all synoptic magnetograms in our data set. **b)** 100-point average of the same data.

4. Pseudo-magnetograms

4.1. Magnetic flux vs. Ca K -line intensity

As the first step in creating pseudo-magnetograms, we considered a correlation between intensity in Ca K line and magnetic flux density. Several previous studies established a power-law relation between the residual intensity in K line and unsigned (line-of-sight) magnetic flux (see Harvey & White 1999; and Ortiz & Rast 2005, and references therein). These studies, however, used moderate-resolution data, typically, 1 by 1 arcsecond pixel size, which corresponds to a resolution lower than 0.1° around equatorial central meridian. Our focus here is on synoptic maps, which have a much larger pixel size, 1 by 1 solar degrees. Figure 5a shows a scatter plot for all pixels in synoptic maps that have both Ca K and magnetogram observations (more than 62 000 points). The data show only a slight noisy trend, but no good correlation between the two parameters. Only after we computed the mean over sequential 100-point segments, a tight dependence between the magnetic flux and residual Ca K-line intensity appears (Fig. 5b). As found in previous studies, the dependence is nonlinear and shows a reversal for areas with the strongest magnetic fields (sunspots).

The data shown in Fig. 5 seem at odds with the previous studies that reported a very strong correlation between the magnetic flux and the residual intensity in the Ca K line. This inconsistency might be explaidn by the fact that we used synoptic maps, which average together multiple pixels from higher resolution full-disk data. Synoptic maps may be constructed from observations made on different days, which reduces correlation even further. Alternatively, it is possible that a tighter correlation is the result of significant averaging. For example, Harvey & White (1999) indicated that for the magnetic flux vs. Ca K residual intensity dependencies they averaged data for different categories of structures over several days to reduce the scatter.

The important question is whether the correlation between magnetic flux and Ca K line intensity is strong or weak. Fortunately, data from the Vector Stokes Magnetograph (VSM) on the Synoptic Optical Long-term Investigation of the Sun (SOLIS) facility (Balasubramaniam & Pevtsov 2011) allow addressing this question. VSM takes full-disk observations of the full line profile in Ca II 854.2 nm. The data can be used to derive cotemporal and cospatial information about the intensity of the chromospheric plages and the magnetic field. The images do not need to be coaligned or corrected for time difference because both parameters are derived from the same spectral line profile. Since the wings of the spectral line are formed in the photosphere and the line core is formed in the chromosphere, the photospheric and the chromospheric magnetograms can both be derived from the same observations. While the response to the magnetic field by intensity in Ca II 854.2 nm spectral line is different from Ca K 393.3 nm, which was used in the historical data sets discussed earlier, this line can serve as a reasonable proxy for Ca K behavior in plages. Figure 6 shows an example of a small portion of a full-disk image observed by SOLIS/VSM on 20 April 2015. Images and magnetograms in the line core (corresponding to the chromosphere) and wing of the spectral line (corresponding to the photosphere) are shown for comparison. The contours outline the sunspots (white), plage and enhanced network (blue), and the brightest parts of the plage (red). The location of plages and intensity enhancements in the Ca II 854.2 nm spectral line correspond very well spatially. Such a one-to-one spatial correspondence was observed before by several researchers (e.g., Cauzzi et al. 2008). A pixel-by-pixel comparison of the magnetic flux density and the normilized intensity (Fig. 7) indicates that while there is a well-defined trend for the plage magnetic field to show a higher intensity for a stronger magnetic flux density, the relation is very noisy. Similar results were found for other observations with SOLIS/VSM.

The significant scatter in the magnetic flux density vs. spectral line core intensity (as observed in the Ca II 854.2 nm spectral line) supports the notion that using intensity as a proxy for the field strength is unreliable. Points corresponding to plage areas

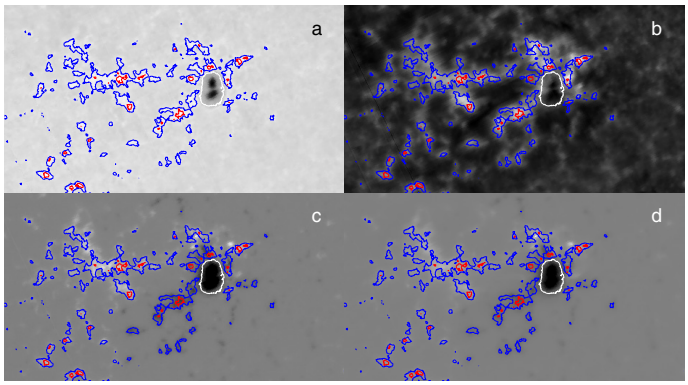

Fig. 6. Image of a solar active region from full-disk observations taken on 20 April 2015 with VSM/SOLIS. Background images correspond to the continuum-normalized intensity in **a)** the wing and **b)** core of the Ca II 854.2 nm line and longitudinal magnetograms corresponding to **c)** the wing (photosphere) and **d)** core (chromosphere). The contours in all panels show the location of sunspots (white, intensity level of 5000 counts), the plage and enhanced network (blue, 5500 counts), and the brightest kernels in the plage (red, 5670 counts). The intensity images were normalized by a limb-darkening function derived directly from the observations. Each panel is about 580 by 537 arcseconds in size, centered on active region NOAA 12324. The background image in panel a is scaled between 2500 and 5800 counts (in comparision, the mean intensity at solar disk center is about 5409 counts). The background image in panel b is scaled between 1800 and 5180 counts (in comparision, the mean intensity at solar disk at line core is about 2670 counts). The magnetograms (background images in panels **c)** and **d)** are scaled between ±1000 G, with white corresponding to positive-polarity fields and black to negative-polarity fields.

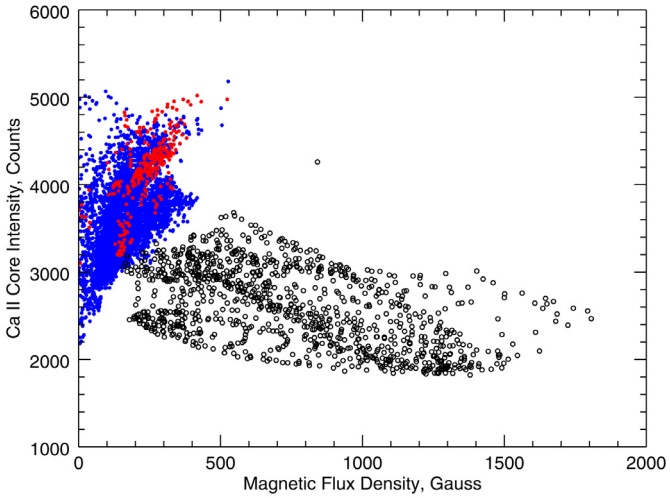

Fig. 7. Scatter plot of the chromospheric magnetic flux density (Fig. 6d) and line-core intensity (Fig. 6b) for sunspot (black) and plage (blue). The brightest plage kernels are shown by red symbols.

may also form two separate branches, one above the other. The upper branch can be identified by the higher concentration of points corresponding to plage kernels (Fig. 7, red on top of blue). Our tests indicated that the upper branch may be related to true plage areas, while the lower branch may represent enhanced network. Qualitatively, this agrees with Harvey & White (1999), who found that the flux-intensity relation has a different steepness for different classes of solar features. Finally, we would like to note that although a core intensity in the Ca II 854.2 nm spectral line can serve as a proxy-magnetometer, this line has specific known issues. For example, the response to the magnetic field

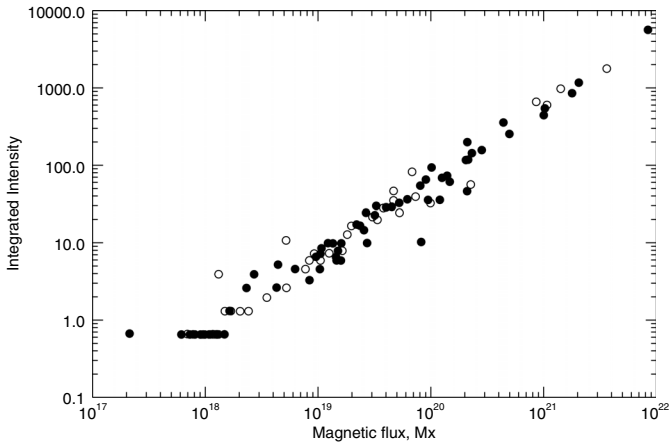

Fig. 8. Plage-integrated intensity as a function of the total unsigned flux. The open circles show data for plage/network elements from observations on 20 April 2015 (shown in Fig. 6) and filled circles show VSM/SOLIS observations from 13 May 2014 .

in this line is susceptible to lower spatial resolution (Leenaarts et al. 2006), which indeed is the case of our VSM/SOLIS observations. Still, we used this line to show the significant scatter in the relation of core intensity vs. magnetic flux density. This level of scatter is present even in the simulations that are unaffected by telescope resolution (see Fig. 4 in Leenaarts et al. 2006).

We therefore propose an alternative scaling of the plage intensity to the magnetic flux using the good correlation between the total magnetic flux in an isolated flux element (plage, enhanced network element) and its integrated brightness. Figure 8 shows such a relation using two examples from VSM/SOLIS observations. For this plot, we identified plages based on an intensity threshold and then integrated intensities and unsigned fluxes within each closed contour above the intensity threshold. This strong correlation can be understood by recalling that the average flux and brightness within plages are independent of the size of a plage, and then the total flux and brightness would be proportional to the total area. For these two cases, the average plage brightness and unsigned flux are approximately constant. This intensity-flux scaling has the additional advantage of preserving the total flux within the area of each plage, even though the flux density is assumed constant within the plage. We find a similar (strong) correlation between the integrated intensity of plages and their total magnetic flux for Ca K synoptic maps and NSO/KP magnetograms.

4.2. Identifying plages and creating pseudo-magnetograms

As the next step, for each synoptic chart we created a mask that identifies plages. The term "chromospheric plage" describes an extended feature that appears brighter than the average chromosphere. Plages are associated with magnetic fields of active regions and appear from the early stages of magnetic flux emergence through its decay. In early stages, plages are well-organized into topologically distinct features, but as they evolve, some parts become barely distinguishable from enhanced chromospheric network. While the plage areas are visually clearly identifiable on full-disk images, their exact boundaries are less clear. An apt analogy for this is a forest boundary where the number of trees and bushes steadily deceases with the distance from the main body of trees. The exact boundary where the forest starts or ends is unclear, and it can only be defined subjectively (e.g., based on density of trees per unit area). This lack of

a clear definition of the boundary of chromospheric plages led some researchers to introduce various subclasses in the attempt to better capture some less obvious differences in the properties of plages. For our current study, we first defined a plage candidate as a linked area of pixels whose brightness is above a fixed intensity threshold. After trial-and-error tests, we adopted a level of two sigma (standard deviation) above the mean intensity of the synoptic map. The threshold is set relatively low, at a typical level of the weak chromospheric network, based on intensity distributions such as shown in Fig. 4 (upper right panel). Next, we analyzed all contours outlining this intensity threshold level in Ca K synoptic maps and excluded obvious artifacts (e.g., chains of pixels with a width of a single pixel, areas located above 75 degrees of latitudes). We also did not count closed contours situated inside other close contours as a separate plage. These areas correspond to dark voids inside bright plages, and excluding them allows us to include the voids as part of larger plage areas (identified by the external contour). Most artifacts are excluded algorithmically, but some may require human intervention. Voids were identified via contours outlining areas situated in bright plages, whose intensity is below the intensity of the surrounding plage.

We identified the polarity of pixels marked as plages based on the polarity of sunspots from the MWO sunspot data set. If the coordinates of a sunspot measurement fall within a plage area, all plage pixels were assigned that polarity. If there are multiple sunspots within the same plage, the pixel polarity within the plage was assigned based on the proximity to each sunspot measurement. This approach allows creating bipolar (or multipolar) structures within a single plage (see Fig, 9, number 2). The weakness of this method is that if the sunspot field strength measurements are incomplete (e.g., only one sunspot in a group was measured), the plage will be incorrectly marked as unipolar (see Fig. 9, number 3) or will not be included in the pseudo-magnetogram (see Fig. 9, number 1). Finally, the amplitude of the magnetic field in the pseudo-magnetogram will be determined using the scaling dependencies between the plage area and the total flux. This scaling preserves the total flux, but the flux density inside the plage is uniform. Figure 9 shows a comparison of observed and pseudo-magnetograms for CR1708. In general, observed and pseudo-magnetograms agree well; in 80% of all pixels that are identified as plages, the polarity of the pseudo-magnetogram agrees well with the observed magnetogram. A pixel-by-pixel comparision between the synoptic pseudo-magnetograms and those from the KPVT computed for 132 Carrington rotations shows a reasonably good correlation, albeit with a significant scatter (Pearson correlation coefficients about $r_P = 0.47–0.50$). This scatter is understandable because of the nonlinear relation between the unsigned magnetic flux and the intensity in the Ca K line (see Fig. 5). On the other hand, the plage-integrated magnetic flux (over each Carrington map) shows a very tight correlation between pseudo- and observed magnetic data ($r_P = 0.98$).

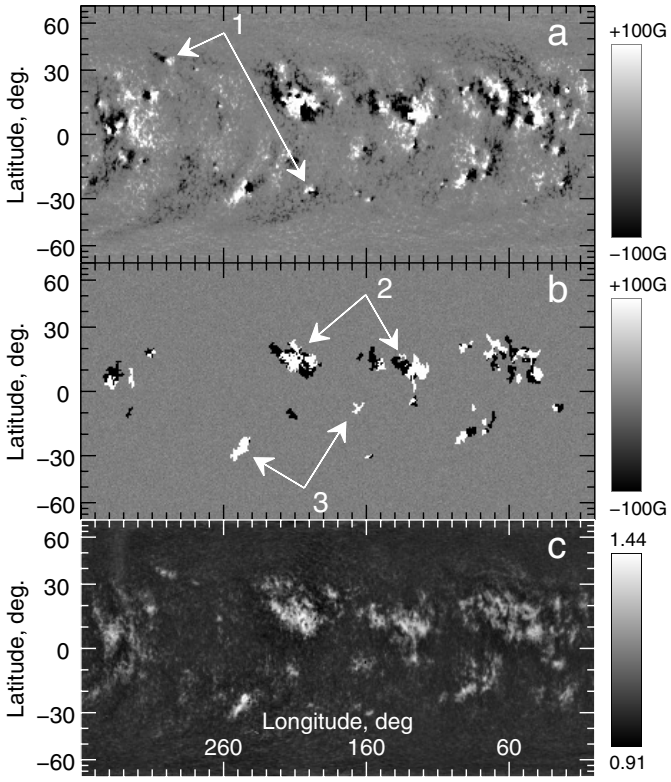

Fig. 9. Observed **a)** and **b)** pseudo-magnetograms and Ca K line **c)** synoptic map of CR1708. Arrows with numbers show examples (1) whithout the active region flux; (2) good agreement between the two; and (3) when only one polarity is present in the pseudo-magnetogram.

5. Discussion and conclusions

We have successfully demonstrated that it is possible to create a homogeneous, long-term series of pseudo-magnetograms using a combination of Ca II K line observations and sunspot polarity measurements. To establish the scaling between the magnetic flux and the intensity in Ca K line spectroheliograms, the spectroheliograms need to be normalized. The original spectroheliograms are nonuniform in their intensity. For example, the chromospheric filaments are clearly seen in synoptic maps taken during some periods, but they are absent from the maps from other periods; the spectroheliograms show higher contrast during cycle 19 than in other periods. Based on existing records from the observer logbooks and previous studies, some key parameters (e.g., spectrograph slit width, optical vignetting, presence of calibration wedge) varied for individual observations. This makes it difficult to properly calibrate the intensities in the entire data set. To mitigate this problem, we developed a different approach. First, we demonstrated that each synoptic map has an intensity pattern, which is related to the chromospheric network (which in turn is related to solar supegranulation). Assuming that the mean properties of this small-scale pattern do not change from one solar rotation to the other, we renormalized the intensities in individual Carrington rotations to fit the Gaussian distribution. For this renormalization, we selected Carrington rotation CR1708 as a standard. This intensity renormalization significantly improved the quality and long-term uniformity of the synoptic maps. For example, the core (shown with blue and yellow in Figs. 2 and 4) becomes much more narrow in the normalized data (compare the width and variations of the core in 1955–1964 in Fig. 2 vs. Fig. 4). The distributions corresponding to different solar maxima (or minima) are more alike to each other (compare the variations and extent of the distribution wings (shown in dark red in Figs. 2 and 4). The quasi-annual variations, which are so distinctive in the original data (see the saw-tooth pattern at the boundary between blue and dark red in Fig. 2 from 1964-1976) are significantly reduced in the normalized data set. This renormalization also affects the overall appearance of large-scale patterns related to the long-term evolution of solar activity. For example, bright features drifting toward the poles (the so-called rush-to-the-poles) during solar

cycle 19 are clearly identifiable in the renormalized data. The original, non-normalized data did not show this feature very clearly. While the intensity normalization improved the quality of the data, it did not completely remove some artifacts, such as quasi-annual variations. We speculate that these quasi-annual variations might be caused by changes in the vignetting pattern at the telescope, and it might be difficult to remove. Nevertheless, we plan to investigate alternative approaches to further improve the Ca K line synoptic data.

The intensity renormalization of Ca K line synoptic maps is based on the assumption that the chromospheric pattern does not change significantly with the solar cycle. Variations in size of the supergranulation were reported by several studies (for review, see Rieutord & Rincon 2010) with somewhat contradictory results. Most studies (e.g., Singh & Bappu 1981) found an anti-correlation with the cycle. Some other studies found the opposite correlation (e.g. Wang 1988; Münzer et al. 1989; Meunier et al. 2008). Tlatov (2012) found a cycle variation in size of the supergranulation with a small phase shift with respect to the sunspot cycle. The phase shift was about 1.5 years, with minima/maxima in the size of the supergranulation occurring after sunspot minima/maxima. We analyzed the annual mean spatial scales detected through a periodogram analysis and found very slight variations over the solar cycle of less then 5%; this is comparable with the scatter of the data points. Thus, we conclude that any possible solar cycle variation in the properties of the chromospheric network are insignificant for the purpose of renormalizing Ca K line synoptic maps.

We showed with the renormalized data that the spatial correspondence between the location of bright areas (plages) and the magnetic field areas in the magnetograms is very good. However, the pixel-by-pixel correlation between the intensity and the magnetic flux is noisy, and thus, a simple scaling of intensities does not provide a good proxy for the amplitude of the magnetic field. This degree of uncertainty is demonstrated in Fig. 5a, where a bright pixel at 1.1 Ca K intensity can correspond to pixels with a magnetic field density from just a few to a thousand Gauss. Data that were a subject to significant averaging demonstrate the nonlinearity of the response of the Ca K line brightness to the magnetic flux: for weak magnetic fluxes (lower than 20−30 Gauss) the flux-intensity correlation is absent, and for the strongest fluxes (higher than a few hundred Gauss) the intensity decreases even when the magnetic flux increases. In this example, the first group of pixels corresponds to magnetic network elements, while the latter represents sunspots. Some of this nonlinearity might be thought to be related to the fact that the magnetogram and Ca K line observations are not simultaneous and are obtained with instruments with different spatial resolution. It appears, however, that this lack of linear correlation is rooted in the physics of the plage: even for cospatial and cotemporal observations, the scatter between magnetic flux and the intensity remains high (Fig. 6). On the other hand, we showed that a good correlation does exist between the total (integrated) intensity and the total unsigned flux within the area of an isolated plage. This suggests that the flux density and the intensity per unit area of plages does not vary significantly between structures of a different size (small and large plages have the same surface brightness and about the same flux density per unit area). This is not unexpected; the modern full Stokes polarimetry observations capable of estimating the contribution from magnetized and non-magnetized plasma in each magnetogram pixel (the so-called magnetic filling factor) indicate that the filling factor in solar plages is about 0.15 (15% of the pixel area corresponds to magnetized plasma), and it does not vary significantly from one plage to another. The strong correlation between plage-integrated intensity and unsigned magnetic flux (Fig. 8) allows us to determine the magnetic flux based on the integral intensity of each plage, although with this approach all pixels within individual plages would be assigned the same magnetic flux density.

Finally, we have shown that a pseudo-magnetogram can be successfully constructed with a combination of sunspot magnetic field polarity measurements and the plages identified from Ca K data. In our tests, about 80% of the pixels situated within plages showed the same magnetic polarity as the synoptic magnetograms taken at the Kitt Peak Vacuum Telescope. In some cases, there is no polarity information for plages either due to lack of sunspot magnetic field measurements or because of there were no sunspots within a plage. To address this problem, we plan on implementing other known properties of solar activity. For example, the Hale-Nicholson polarity rule indicates that in most cases, the leading polarity of bipolar regions in a given cycle is determined by their hemispheric location. Different studies have found that only between 1.4% and 9.1% of all active regions do not follow this rule (for a review, see Pevtsov et al. 2014), and thus, the polarity in the leading and following parts of the plage might be determined with a high degree of success by implementing this approach.

In conclusion: we employed the Carrington maps of CaII K line data taken at Mount Wilson Observatory from 1915–1985 to identify the chromospheric plages and to create synoptic pseudo-magnetograms. We used historical observations of the polarity of sunspot magnetic fields from 1917 to the present to assign polarity to pixels situated within plages. Using the intensity as a proxy for the unsigned flux density requires renormalizing original Ca K line observations, for which we developed a new approach based on the properties of the Gaussian core of the intensity distributions of these data. We successfully demonstrated that a homogeneous long-term series of pseudo-magnetograms can be constructed with this approach. We will apply pseudo-magnetograms to study the solar phenomena in future papers.

Acknowledgements. National Solar Observatory is operated by the Association of Universities for Research in Astronomy (AURA), Inc. under a cooperative agreement with the National Science Foundation. We acknowledge the financial support by the Academy of Finland to the ReSoLVE Centre of Excellence (project no. 272157). This work utilizes data acquired by SOLIS/VSM operated by NISP/NSO/AURA/NSF. A.A.P. thanks the faculty and students of ReSoLVE Centre of Excellence of University of Oulu for their hospitality during his long-term visit. The authors thank the anonymous referee for the constructive comments that improved this article.

References

Babcock, H. W., & Babcock, H. D. 1955, ApJ, 121, 349
Balasubramaniam, K. S., & Pevtsov, A. A. 2011, Proc. SPIE, 8148, 814809
Bertello, L., Ulrich, R. K., & Boyden, J. E. 2010, Sol. Phys., 264, 31
Cauzzi, G., Reardon, K. P., Uitenbroek, H., et al. 2008, A&A, 480, 515
Ellerman, F. 1919, PASP, 31, 16
Foukal, P., Bertello, L., Livingston, W. C., et al., 2009, Sol. Phys., 255, 229
Hale, G. E. 1908, ApJ, 28, 244
Hale, G. E., Ellerman, F., Nicholson, S. B., & Joy, A. H. 1919, ApJ, 49, 153
Harvey, K. L., & White, O. R. 1999, ApJ, 515, 812
Hathaway, D. H. 2010, Liv. Rev. Sol. Phys., 7, 1
Hyder, C. L. 1965, ApJ, 141, 272
Leenaarts, J., Rutten, R. J., Carlsson, M., & Uitenbroek, H. 2006, A&A, 452, L15
Leighton, R. B. 1959, ApJ, 130, 366
Livingston, W. C., Harvey, J., Slaughter, C., & Trumbo, D. 1976, App. Opt., 15, 40

Meunier, N., Roudier, T., & Rieutord, M. 2008, A&A, 488, 1109
Münzer, H., Schröter, E. H., Wöhl, H., & Hanslmeier, A. 1989, A&A, 213, 431
Ortiz, A., & Rast, M. 2005, Mem. Soc. Astron. It., 76, 1018
Pesnell, W. D. 2014, Sol. Phys., 289, 2317
Petrovay, K. 2010, Liv. Rev. Sol. Phys., 7, 6
Pevtsov, A. A., Nagovitsyn, Y., Tlatov, A., & Rybak, A. 2011, ApJ, 742, L36
Pevtsov, A. A., Berger, M. A., Nindos, A., Norton, A. A., & van Driel-Gesztelyi, L. 2014, Space Sci. Rev., 186, 285
Pishkalo, M. I. 2014, Sol. Phys., 289, 1815
Rieutord, M., & Rincon, F. 2010, Liv. Rev. Sol. Phys., 7, 2
Singh, J., & Bappu, M. K. V. 1981, Sol. Phys., 71, 161
Stepanov, V. E., & Petrova, N. N. 1959, Bull. Crimean Astrophys. Obs., 21, 152
Tlatov, A. G. 2012, in The Sun: New Challenges, Astrophys. Space Sci. Proc., 30, 33
Tlatov, A. G., & Pevtsov, A. A. 2010, Mem. Soc. Astron. It., 81, 814
Tlatov, A. G., Pevtsov, A. A., & Singh, J. 2009, Sol. Phys., 255, 239
Tlatov, A. G., Tlatova, K. A., Vasil'eva, V. V., Pevtsov, A. A., & Mursula, K. 2015, Adv. Space Res., 55, 835
Wang, H. 1988, Sol. Phys. 117, 343
Upton, L., & Hathaway, D. H. 2014, ApJ, 792, 142